frontiers in Earth Science

ORIGINAL RESEARCH
published: 12 June 2020
doi: 10.3389/feart.2020.00176

Allometric and Phylogenetic Aspects of Stapes Morphology in Ruminantia (Mammalia, Artiodactyla)

Bastien Mennecart[1], Coraline Guignard[1], Laura Dziomber[2], Georg Schulz[3,4], Bert Müller[3] and Loïc Costeur[1]*

[1] Naturhistorisches Museum Basel, Basel, Switzerland, [2] Institute of Plant Sciences and Oeschger Centre for Climate Change Research, University of Bern, Bern, Switzerland, [3] Biomaterial Science Center, University of Basel, Allschwil, Switzerland, [4] Department of Biomedical Engineering, Micro- and Nanotomography Core Facility, University of Basel, Allschwil, Switzerland

The stapes is the smallest bone of the mammalian skeleton. Being the innermost middle ear ossicle, it is in contact with the inner ear and is directly responsible for sound transmission into it. Today, Ruminantia are one of the most diversified groups of large mammals with more than 200 species. However, their stapes has been very little studied. Here we investigate the shape of 66 stapes from 44 species of extant and extinct Ruminantia, including intra-individual and intra-specific observations, based on 3D tomographic data. Shape differences and similarities are quantitatively discussed thanks to 3D geometric morphometrics. The overall size of the stapes scales with a negative allometry in comparison to body mass. Moreover, the overall shape of the stapes informs about phylogeny. A trend is observed from a concave posterior crus with an enlarged stapes capitulum in Antilocapridae to a relatively straight posterior crus with a little reduced stapes capitulum in Cervidae, Bovidae being intermediate. In addition, the stapes of Antilocapridae is relatively trapezoid in lateral view; that of Cervidae is more triangular in lateral view; and that of Bovidae is relatively rectangular in lateral view. The stapedial footplate shape also gives phylogenetic information. The Tragulidae stapedial footplate is antero-posteriorly asymmetrical. The stapedial footplate is ovoid in stem Pecora. It is asymmetrical in Bovidae, while it is more symmetrical in Cervidae. This is in agreement with previous studies on the ruminant bony labyrinth showing that the oval window, the counterpart of the stapedial footplate on the inner ear, bears a strong phylogenetic signal already distinguishable in early Miocene ruminants.

Keywords: geometric morphometrics, ear region, systematics, middle ear ossicles, micro computed tomography

OPEN ACCESS

Edited by:
Pasquale Raia,
University of Naples Federico II, Italy

Reviewed by:
Saverio Bartolini Lucenti,
University of Florence, Italy
Antonio Profico,
Sapienza University of Rome, Italy

****Correspondence:***
Bastien Mennecart
mennecartbastien@gmail.com

Specialty section:
This article was submitted to Paleontology, a section of the journal Frontiers in Earth Science

Received: *18 December 2019*
Accepted: *06 May 2020*
Published: *12 June 2020*

Citation:
Mennecart B, Guignard C, Dziomber L, Schulz G, Müller B and Costeur L (2020) Allometric and Phylogenetic Aspects of Stapes Morphology in Ruminantia (Mammalia, Artiodactyla). Front. Earth Sci. 8:176. doi: 10.3389/feart.2020.00176

INTRODUCTION

The middle ear bones (ossicles) compose a chain of three bones (stapes, incus, and malleus) forming a complex structure only present in mammals. These bones play a central role in air-borne sound transmission from the outer environment to the inner ear (Merchant et al., 1996). The evolution of the incus and the malleus from the "reptilian grade" jaw bones to the smallest bones of the mammalian skeleton has been intensively studied (e.g., Rich et al., 2005; Luo, 2007; Meng et al., 2011; Maier and Ruf, 2016a,b). Their morphology and size are often associated to hearing sensitivity (Fleischer, 1978; Rosowski and Graybeal, 1991; Stoessel et al., 2016a; Bernardi and Couette, 2017).

However, only a few recent studies (except for Primates and aquatic mammals) focused on intraspecific variability or searched for phylogenetic characters potentially borne by this structure (e.g., Maier and Ruf, 2016b; Orliac and Billet, 2016; Bastl et al., 2017). The stapes is directly in contact with the inner ear through the stapedial fenestra or oval window. This bone can be well-preserved in fossil specimens where it can be found "fallen in a dead ear" as put by Orliac and Billet (2016). The stapes morphology is quite conservative among placental mammals (Fleischer, 1978). Nevertheless, the three dimensional (3D) structure of this bone is complex and can barely be described based on 2D images only (Stoessel et al., 2016b).

Ruminantia, hereafter also referred to as "ruminants," are one of the most diverse clades of large mammals, with more than 200 extant species living from the boreal tundra (e.g., reindeer) to the tropical forest (e.g., mouse deer), and the high mountains (e.g., Himalayan tahr; Nowak, 1999). Their social behavior ranges from solitary to gregarious. This diversity in ruminant ecology makes them a perfect case study for the investigation of ossicle ecomorphology. However, except for Fleischer (1973) and Maier and Ruf (2016b), there is almost no new data on the morphology of ruminant ossicles since Hyrtl (1845), Doran (1878), and Wilkie (1925, 1936). Costeur et al. (2016) described the ossification timing and the morphology of the ossicles in a mid-gestation cow fetus. The stapedial footplate does not reach its adult size at this stage contrary to the inner ear and its oval window articulating with the stapes (Costeur et al., 2016, 2017).

Here we describe the morphology of ruminant stapes covering all extant families and several fossil examples spanning 25 million years of ruminant evolution. Specific statistical analyses on the stapes shapes are performed in order to assess the impact of evolutionary allometry and phylogenetic inheritance on the morphology of this poorly studied middle-ear ossicle.

MATERIALS AND METHODS

Material

Sixty-six stapes from 44 species of ruminants were reconstructed from micro computed tomography data. The dataset includes Tragulidae (two extant species and one fossil from the early Miocene), stem Pecora (3 species from the latest Oligocene to early Miocene), and crown Pecora: Antilocapridae (3 species from the Pleistocene to recent), Bovidae (21 extant species), Cervidae (12 species from the early Miocene to recent), Giraffidae (1 extant species), and Moschidae (1 extant species; see **Table 1**). The bones from extant species are extracted from dry specimens of the Naturhistorisches Museum Basel (NMB, Switzerland). The fossil specimens exclusively came from Eurasia and America and are stored in Swiss, German, British, and American institutions (**Table 1**). To observe the intra-individual variability of the bone, the left and right stapes of the Bovidae *Aepyceros melampus* (NMB 9017), *Bubalus depressicornis* (NMB 3269), *Redunca fulvorufola* (NMB 15091), and *Gazella gazella* (NMB 11029); of the Cervidae *Elaphodus cephalophus* (NMB 2067) and *Muntiacus muntjak* (NMB C.2408); and of the Tragulidae *Hyemoschus aquaticus* (NMB 2692) and *Tragulus kanchil* (NMB 2131, NMB 2988, and NMB 3795) were reconstructed and compared. Similarly, insights into intraspecific variability is given through limited samples for the fossil Cervidae *Dicrocerus elegans* (2 specimens) and *Procervulus praelucidens* (2 specimens) and the fossil Pecora *Dremotherium feignouxi* (2 specimens) and quantified in the fossil Antilocapridae *Capromeryx arizonensis* (3 specimens), as well as 8 Tragulidae *Tragulus kanchil*.

Institutional Abbreviations

AMNH: American Museum of Natural History, New York (United States); MHNT: Muséum d'histoire naturelle de Toulouse (France); NHMUK: Natural History Museum of United Kingdom, London (United Kingdom); NMB: Naturhistorisches Museum Basel (Switzerland); and UF: Florida Museum of Natural History – University of Florida in Gainesville (United States).

Measurements and Nomenclature

The body mass and bony labyrinth length of the extant ruminants are adapted from Nowak (1999), and Wilson (2005) for the duikers (*Cephalophus dorsalis* and *Cephalophus zebra*). The stapes anatomical nomenclature is given on **Figure 1**.

CT-Scanning and Reconstruction

The specimens were scanned using high resolution hard X-ray computed tomography using nanotom® m (phoenix|x-ray, GE Sensing & Inspection Technologies GmbH, Wunstorf, Germany). Pixel resolution varies between 15 and 60 μm. During each aquisition 1440 equiangular radiographs were taken over 360° using an accelerating voltage of 90 kV and a beam current of 200 μA for recent material and 180 kV with a beam current of 30 μA for fossils. Segmentation of the stapes was done with AVIZO®9.0 Lite software (Visualization Sciences Group).

Morphometrics Analyses

The main objectives of this article are to characterize the allometry (both in size and shape) and the phylogenetical aspects of the stapes morphology in ruminants.

To quantify size allometry, resulting statistics based on linear measurements were performed with the PAST 4.0 software (Hammer et al., 2001). The correlation interface of the univariate analyses allows testing the relationship between the stapes (volume), the body mass (volume), the bony labyrinth (length), and different stapes parts (surface) using Linear r (Pearson) and p(uncorr) parameters based on decimal logarithm of the values (**Supplementary Data S2**). The weight (W) and length (L) relationships are $W = a \times L^{\alpha}$ or $\log(W) = \log(a) + \alpha \times \log(L)$ (Shingleton, 2010; Karachle et al., 2012). "α" is the slope of the correlation. In an isometric context, "α" is the coefficient balancing the dimensions of the equation (Karachle et al., 2012). Its isometrical values depends on the dimension of the compared data (length vs volume or mass, α = 3/1 when isometric; surface vs volume, α = 3/2 when isometric). When α > isometric value, there is a positive allometry of the first independent variable in comparison to the second dependent one. When α < isometric value, there is a negative allometry of the first variable in comparison to the second one (Shingleton, 2010).

TABLE 1 | List of studied specimens.

Family	Sub-family	Species	Inventory number	Age (Ma)
"stem Pecora"	–	*Parablastomeryx gilchristensis*	UF265266	19–17.5
	–	*Dremotherium feignouxi*	NMBMA5885	21
	–	*Dremotherium feignouxi*	NMBMA5886	21
	–	*Amphitragulus feningrei*	NMBcod632	24
Antilocapridae	Antilopinae	*Antilocapra americana*	NMBC1618	0
		Capromeryx arizonensis	UF402857*	2
		Capromeryx arizonensis	UF402858	2
		Capromeryx arizonensis	UF402859*	2
		Stockoceros onusrosagris	AMNHFAM 42553*	1.8–0.01
Giraffidae	–	*Giraffa camelopardis*	NMB2197	0
Cervidae	Cervinae	*Procervulus praelucidens*	MHNT.PAL. 2015.02385	16.5
		Procervulus praelucidens	MHNT.PAL.2015 .0226114*	16.5
		Dicrocerus elegans	NMBSan1001	15
		Dicrocerus elegans	NMBSan1003	15
		Elaphodus cephalophus	NMB2067.1	0
		Elaphodus cephalophus	NMB2067.2*	0
		Muntiacus muntjiak	NMBC2408.1	0
		Muntiacus muntjiak	NMBC2408.2*	0
		Rusa timorensis	NMB3657	0
		Rusa unicolor	NMB9597*	0
		Cervus nippon	NMB6106	0
	Capreolinae	*Hydropotes inermis*	NMB9892*	0
		Mazama americana	NHM.UK. PVOR.18701*	0
		Odocoileus sp.	UF402856*	2
		Mazama gouazoubira	NMB6672	0
		Ozotoceros bezoarticus	NMB2312*	0
		Pudu puda	NMBC2209	0
Moschidae	–	*Moschus moschiferus*	NMB8874	0
Bovidae	Bovinae	*Tragelaphus sciptus*	NMBC3568	0
		Bubalus depressicornis	NMB3269	0
		Bubalus depressicornis	NMB3269*	0
		Tetracerus quadricornis	NMB10472*	0
		Boselaphus tragocamelus	NMB10258	0
	Antilopinae	*Neotragus moschatus*	NMBC2122	0
		Aepyceros melampus	NMB9017.1	0
		Aepyceros melampus	NMB9017.2*	0
		Gazella gazella	NMB11029.1	0
		Gazella gazella	NMB11029.2*	0
		Gazella subgutturosa	NMB2497	0
		Eudorcas albonotata	NMB6414	0
		Redunca fulvorufula	NMB15091.1	0
		Redunca fulvorufula	NMB15091.2*	0
		Damaliscus pygargus	NMBC1948*	0
		Connochaetes gnou	NMB7591	0
		Ovis aries	NMB9037	0
		Rupicapra pyrenaica	NMBC1830*	0
		Ammotragus lervia	NMB2084*	0
		Capra hircus	NMB6920	0
		Ovibos moschatus	NMB11175	0
		Oreotragus oreotragus	NMBC4228*	0
		Oreotragus oreotragus	NMB8401*	0
		Cephalophus dorsalis	NMB15928	0
		Cephalophus zebra	NMBC2784	0
Tragulidae	–	*Dorcatherium crassum*	MHNT.PAL. 2015.02707*	16.5
		Hyemoschus aquaticus	NMB2692.1	0
		Hyemoschus aquaticus	NMB2692.2*	0
		Tragulus kanchil	NMB2131.1	0
		Tragulus kanchil	NMB2131.2	0
		Tragulus kanchil	NMB2988.1	0
		Tragulus kanchil	NMB2988.2	0
		Tragulus kanchil	NMB3791	0
		Tragulus kanchil	NMB3795.1	0
		Tragulus kanchil	NMB3795.2	0
		Tragulus kanchil	NMB3797	0
		Tragulus kanchil	NMB3806	0
		Tragulus kanchil	NMBC3802	0
		Tragulus kanchil	NMBC3735*	0

*Specimen with * have been mirrored for the analysis.*

Digitization of the stapes was performed using Landmark Editor 3.6 software (Wiley, 2006). In addition to the landmarks proposed in Stoessel et al. (2016b), we have landmarked the shape of the stapes capitulum (*capitulum stapedis*), the anterior crus (*crus anterius stapedis*), and the posterior crus (*crus anterius stapedis*; **Figure 1**). Eight landmarks of type 2 identify the maximum length of the stapes capitulum and the stapedial footplate (*basis stapedis*) and the maximum height of both intercrural foramens (**Figure 1**). Curves (each containing 10 equidistant semi landmarks) are placed on the stapes: two curves surrounding the stapedial footplate, two curves surrounding each intercrural foramen, one curve on each crus (anterior and posterior on their medial part), two curves surrounding the stapes capitulum.

We tested the correlation between the shape of the stapes and its size using a regression of the shape on the centroid size as defined by Klingenberg (2016) as "the square root of the sum of squared distances of all the landmarks of an object from their centroid [center of gravity, whose location is obtained by averaging the x and y (and z) coordinates of all landmarks]."

The correlation between two shape modules of the stapes has been tested using the modularity implementation of MorphoJ 1.06d software (Klingenberg, 2011). Morphological modules are parts whose components covary strongly, but which are relatively independent of other modules (e.g., Klingenberg, 2008). We have chosen to separate two modules. We have defined as a first module both crurae stapedis since they have a similar embryologic origin. The second module is the remaining set of landmarks. 1.000.000 random partitions have been considered using (**1**) the original dataset, (**2**) the dataset without allometrical signal, and (**3**) the dataset without allometrical signal pooled by family as explained afterward.

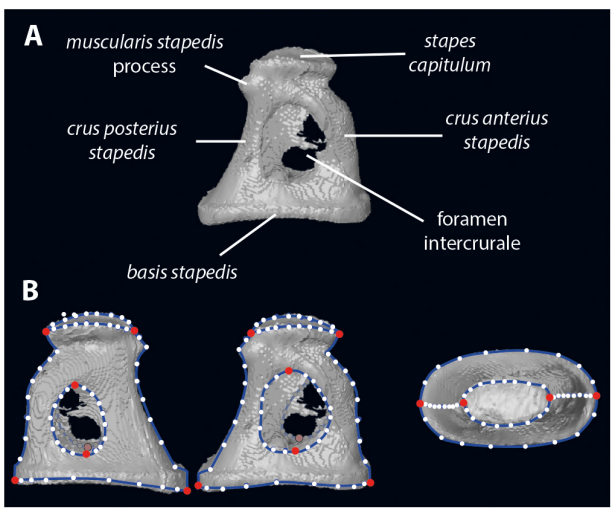

FIGURE 1 | Stapes morphology (based on *Hydropotes inermis* NMB 9892). **(A)** anatomical nomenclature; **(B)** landmark set (in red landmarks of type 2 and white semilandmarks on blue curves). 3D specimen is in **Supplementary Data S1**.

Shape variation in stapes morphology (disparity and similarity) was studied using a geometric morphometrics approach implemented in MorphoJ and R. To explore the phylogenetical relevance of this structure, we have created three datasets to characterize the shape of the stapes using (**1**) the original dataset (with allometrical signal), (**2**) a dataset without allometrical signal not pooled by family (since a significant correlation between the shape of the stapes and its size exists, p-values = 0.0018, see section "Phylogenetic signal", and **Supplementary Data S3**), and (**3**) a dataset without allometrical signal pooled by family (since a significant correlation between the size of the stapes and its phylogeny exists, p-values = 0.0235, see section "Phylogenetic signal", and **Supplementary Data S3**). As mentioned by Klingenberg (2016): "Pooled within-group (here the families) regression uses the shape and size deviations of each specimen from the shape and size averages of the group to which that specimen belongs (here the families), not the grand mean, to compute variances and covariances (. . .). Equivalently, pooled within-group regression can be explained as a two-step procedure where the differences among group averages are first removed by centering the shape and size data by group and then an ordinary regression is carried out on these centered data." Working on residual values allows an exploration of the dataset with non-allometric variation (Klingenberg, 2016) and to focus here on phylogenetical parameters.

The principal component analysis (PCA) is used on the three datasets (**1** original dataset, **2** dataset without allometrical signal, and **3** dataset without allometrical signal pooled by family) to visualize the overall shape variation among specimens. A permutation test (randomized rounds: 10.000; Klingenberg and Gidaszewski, 2010) based on the phylogenetic tree (**Supplementary Data S4**) is performed to test the presence or absence of a phylogenetic signal in the three datasets. Klingenberg and Gidaszewski (2010) defined that "The empirical p-value for the test is the proportion of permuted data sets in which the sum of squared changes is shorter or equal to the value obtained for the original data." Marriott (1979) and Edgington (1987) suggested that 1.000 permutations are a reasonable minimum for a test at 5% level of significance, while 5.000 are a reasonable minimum at the 1% level (Tzeng and Yeh, 1999). The phylogenetic tree was manually created using Mesquite 3.04 software (Maddison and Maddison, 2010) combining tree hypothesis published by Janis et al. (1998), Hassanin et al. (2012), Mennecart (2012), and Mennecart et al. (2019). Time calibration was provided by Bibi (2013) and Mennecart et al. (2017). Since it is difficult to observe the "geographical" proximity of two individuals within a polymorphospace including more than 4 dimensions, a hierarchical analysis using the cluster analysis option of the PAST 4.0 software (Hammer et al., 2001) has been performed (**Supplementary Data S2**). This allows observing graphically, along a tree, shape distances between specimens. Using the Euclidean similarity value option of PAST considering that the Procrustes coordinates, the Euclidean distances can directly be assimilated to Procrustes distances.

To characterize the phylogenetical differences of the stapes among the different ruminant families, standardized discriminant analyses have been performed.

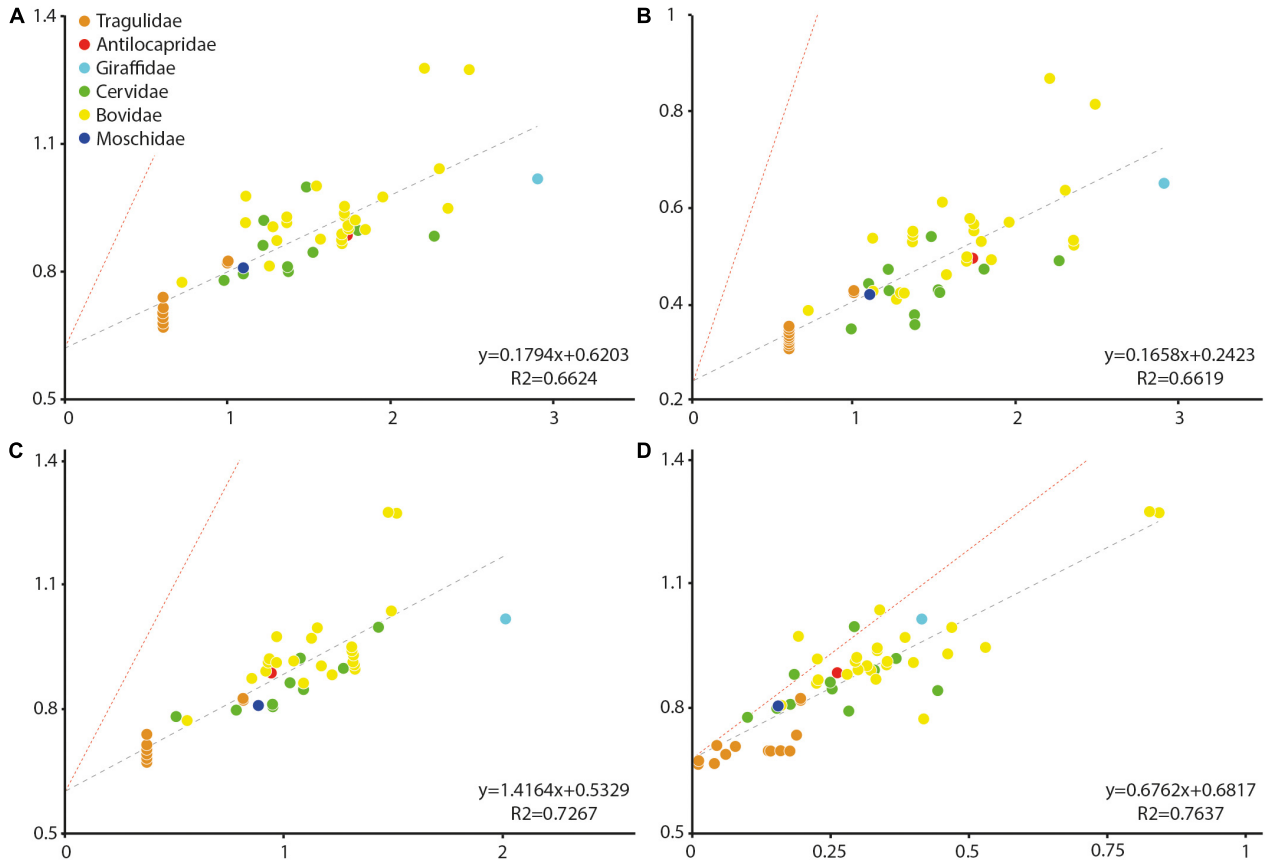

FIGURE 2 | Size allometry of the stapes structures in comparison to body mass in living ruminants, to other stapes structures, and to bony labyrinth length. **(A)** body mass against stapes centroid size; **(B)** body mass against the stapedial footplate centroid size; **(C)** bony labyrinth length against stapes centroid size; and **(D)** intercrural foramen centroid size against stapes centroid size. All values are in log. Antilocapridae red; Bovidae, yellow; Cervidae, green; Tragulidae, orange; Giraffidae, and light blue; Moschidae, dark blue. Red line corresponds to isometry.

A between-group PCA (bg-PCA) has been performed based on the three above mentioned datasets using the package *Morpho* (Schlager, 2017) in R (R Core Team, 2005) with the function "groupPCA." Contrary to the following Canonical Variate Analysis (CVA), a bg-PCA observes the variance between groups (here the well-defined ruminant families Tragulidae, Cervidae, Bovidae, and Antilocapridae and the stem Pecora) without standardizing the within groups-variance (Renaud et al., 2015). It gives less pressure on the shape similarities within group. Moschidae and Giraffidae have been excluded of the analyses since only one specimen (*Moschus moschiferus* and *Giraffa camelopardis*, respectively) possesses a well-preserved stapes. All supporting data of the bg-PCA (script and supporting information) can be found in **Supplementary Data S5**. Recent studies have cautioned the use of bg-PCA in high dimensional datasets (e.g., Cardini et al., 2019) but as reminded by Cardini et al. (2019) the common feature of correlated data in geometric morphometrics helps to circumvent this problem.

Additionally, the CVA was applied on the three above mentioned datasets to maximize the separation of the between-group means relative to the variation within groups ratio according to the specified chosen grouping variable (Renaud et al., 2015). CVA and bg-PCA provides complementary information (Mitteroecker and Bookstein, 2011; Renaud et al., 2015). Nevertheless, due the high degree of freedom in our analysis, CVA can be found in **Supplementary Data S6** as a comparative dataset (**Supplementary Data S3** presenting the results and 6 including figure and supporting information).

All statistical reports are shown in the **Supplementary Data S2, S3, S5**.

RESULTS

Allometric Signal

Stapes centroid size and stapedial footplate centroid size (in decimal logarithm of the values) are correlated with body mass (R^2 = 0.6624, p-value < 0.0001 and R^2 = 0.6619, p-value < 0.0001, respectively). A strong negative allometry is observed between these elements and body mass (α = 0.1794 and α = 0.1658, respectively, a isometry values being 1 and 1.5, respectively, **Figure 2**) indicating that larger species have relatively small stapes and smaller species have relatively large ones. The scaling relationship between the stapes centroid

size and its bony labyrinth length is positively allometric (α = 1.4164, a isometry values being 0.333) with a clear correlation (R^2 = 0.7267, p-value < 0.0001). The intercrural foramen centroid size and the stapes centroid size are correlated (R^2 = 0.7637, p-value < 0.0001). The intercrural foramen centroid size possesses a negative allometry in comparison to the stapes centroid size (α = 0.6762, a isometry values being 1.5) indicating that the intercrural foramen grows slower than the stapes (**Figure 2**).

To study the covariation between the shape and size, regressions of the shape (Procrustes coordinates) on the centroid size have been performed, both un-pooling and pooling the dataset by families. The not pooled dataset gives a statistically significant result (p-value = 0.0018, **Supplementary Data S3**) indicating a correlation between the size and the shape of the stapes (**Figure 3**). The effect size is nonetheless small, being R-squared at 0.037. Similar statistical results are observed when pooling the dataset by family (p-value = 0.0037 and a shape prediction at 3.46%). The main shape deformations observed in both analyses are the size of the intercrural foramens relative to the stapes size and the relative size of the stapedial footplate. In small forms, the two intercrural foramens are of similar size and relatively small (1/2 to 2/3 of the height of the stapes in the not pooled analysis and 1/2 for both intercrural foramens in the pooled analysis). Their stapedial footplate is more than twice as long as the stapes capitulum and relatively symmetrical. In large forms (*Ovibos moschatus* and *Connochaetes gnou*), one intercrural foramen remains relatively small and the second one almost entirely occupies the space between the stapes capitulum and the footplate, extending antero-posteriorly almost reaching the crura stapedis. Their stapedial footplate is smaller than twice the stapes capitulum length, the capitulum being wider in the pooled data (**Figure 3B**). The shape differences between the two analyses are mainly located on the shape of the stapedial footplate. While in the not pooled result the stapedial footplate is very asymmetrical with one side being flattened, in the pooled data, the stapedial footplate is only slightly asymmetrical. The two largest stapes of the dataset belong to Bovidae and all the smallest stapes belong to Tragulidae. A significant correlation between the size of the stapes and its phylogeny exists considering the unpooled dataset, (p-values = 0.0235, section "Phylogenetic signal", **Supplementary Data S3**). This informs that bovids do possess an asymmetrical stapedial footplate that is phylogenetically relevant.

Modularity

The determination of the different modules based on the three datasets containing the entire stapes (original data and after correction of the size effect without pooling and pooled by family) leads to similar results. The minimal RV coefficient calculated among the 1.000.000 partitions evaluated is 0.461519 for the original dataset, 0.467736 for the dataset with correction of the size effect, and 0.482582 for the dataset with correction of the size effect pooled within families. In each case, the two modules are "capitulum + stapedial footplate + crura stapedis" and "intercrural foramens" as in the original hypothesis (**Figure 3C**). There is no alternative partition with an RV coefficient smaller or equal to the value for the hypothesis (proportion is equal to 0.000). It is interesting to note that the crurae stapedis have a similar embryologic origin, forming at the end a hollow structure. The rest of the structure is made of bone: the capitulum and the stapedial footplate are the most massive bone portion of the stapes. These relatively flattened sections receive and transmit pressure perpendicular to their surface thanks to the crura stapedis.

PCA

Very little morphological variation is observed between the left and right stapes of a same individual. Observing the hierarchical analysis result, most of the left stapes cluster with their right counterpart (see hierarchical analysis in **Supplementary Data S2**). Similarly, a very weak intraspecific variability is observed. Most of the *Tragulus kanchil* cluster together associated to the other Tragulidae *Hyaemoschus aquaticus* (**Supplementary Data S2**). Similarly, the two duiker species (*Cephalophus dorsalis,* and *Cephalophus zebra*) cluster together (**Supplementary Data S2**) indicating that the entire shape of the stapes may provide phylogenetical information.

The shape disparity and the morphospace of the studied samples are very similar in all the three datasets (**1** original dataset, **2** dataset without allometrical signal (not pooled by family), and **3** dataset without allometrical signal pooled by family), the PC2 axis being mirrored in the results without size effect in comparison to original dataset (**Figure 4**). The changes mostly concern the position of the two large stapes (*Ovibos moschatus* and *Connochaetes gnou*). Considering the original dataset, the dataset without allometrical signal, and the dataset without allometrical signal pooled by family, the maximum of variance along PC1 (13.75, 13.87, and 13.86% of the variance, respectively) goes from a massive and short stapes in the negative values to a slender and elongated one in the positive values. The stapes capitulum and the stapedial footplate are enlarged with short crura stapedis in PC1 negative values. Their intercrural foramens are relatively rounded and central. The stapedial footplate is ovoid to slightly elongate. The stapes capitulum and the stapedial footplate are short with elongated crura stapedis in positive PC1 values. Their intercrural foramens are ovoid and the space between the intercrural foramens and the anterior crus is narrow. The stapedial footplate is ovoid and short. PC2 explains 9.14, 9.21, and 10.20% of the variance of the original dataset, the dataset without allometrical signal, and of the dataset without allometrical signal pooled by family, respectively. In the negative PC2 values based on the original dataset, the intercrural foramens are a little closer to the stapedial footplate, but the general shape is very similar to the consensus shape (**Figure 4**). Considering the PC2 positive values based on the original dataset, the height of the stapes is similar to the consensus but the latter is a little narrower. The intercrural foramens are very elongated and closer to the posterior crus. The negative and positive PC2 shape variations are inverted in the datasets without allometrical signal (not pooled and pooled by family) in comparison to the original dataset. The shape of the stapedial footplate is different along the PC2 axis between

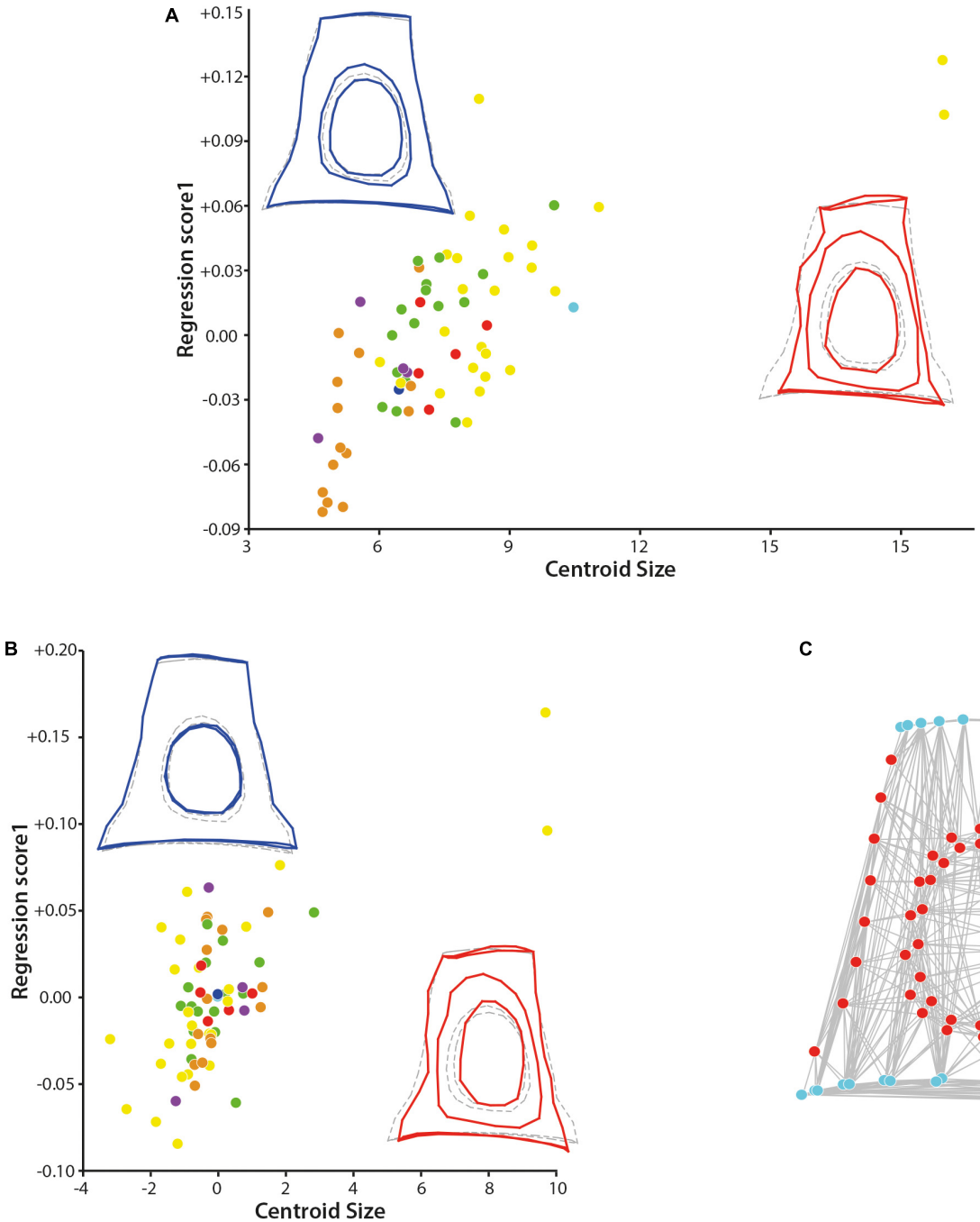

FIGURE 3 | Results of the regression on the centroid size and of the modularity test. **(A)** Regression of the shape of the stapes on the centroid size and **(B)** regression of the shape of the stapes on the centroid size pooled within families. **(C)** Result of the modularity test (similar to the original hypothesis) on the original 3D landmarks dataset, the stapes with size correction dataset, and the stapes with size correction pooled within families (all three analyses give similar result, graph shows the first result, the two others are not shown). Stem Pecora violet; Antilocapridae red; Bovidae, yellow; Cervidae, green; Tragulidae, orange; Giraffidae, and light blue; Moschidae, dark blue. Statistical results are available in **Supplementary Data S3**.

pooled data on one side and the original dataset and the not pooled ones on the other side (PC2 shape variation of the original data being mirrored in comparison to the not pooled one). The negative values of PC2 in the pooled dataset show a drop-like shape of the surface area of the stapedial footplate. Considering the not pooled data negative PC2 values (positive ones for the original data), the stapes is ovoid and more symmetrical. On the other end of PC2 axis, the stapedial footplate is ovoid and more asymmetrical in all three datasets. However, the asymmetry is more marked from the original dataset to the dataset after size

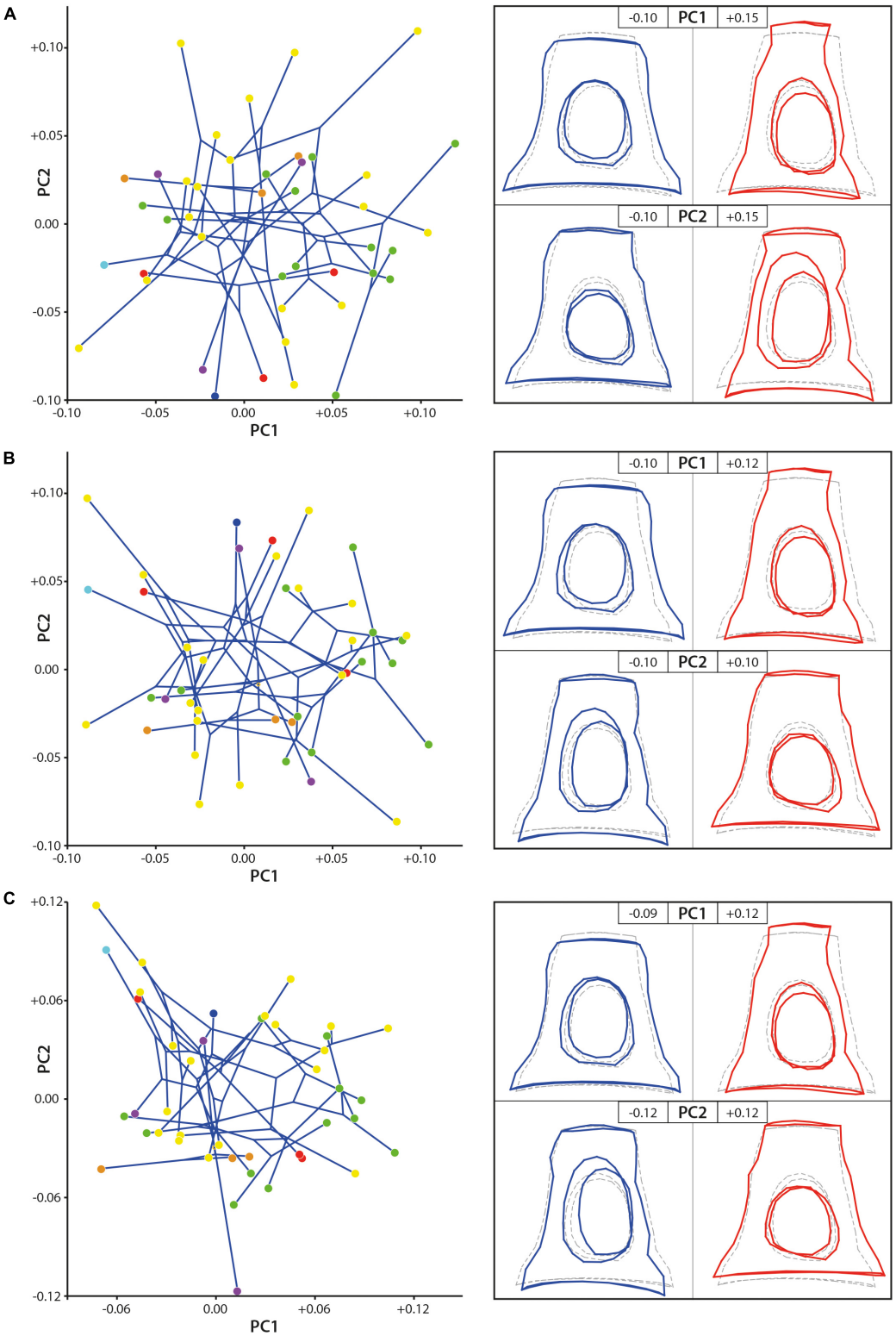

FIGURE 4 | Geometric morphometric PCA results. **(A)** stapes based on the original 3D landmarks coordinates (dataset 1; PC1 = 13.75%, PC2 = 9.14%), **(B)** dataset without allometrical signal not pooled by family (dataset 2; PC1 = 13.87%, PC2 = 9.21%), and **(C)** dataset without allometrical signal pooled by family (dataset 3; PC1 = 13.86%, PC2 = 10.20%). The morphological modifications along the axes (PC) are materialized by the hypothetical stapes shape associated to extreme values. Stem Pecora violet; Antilocapridae red; Bovidae, yellow; Cervidae, green; Tragulidae, orange; Giraffidae, and light blue; Moschidae, dark blue. Statistical results are available in **Supplementary Data S3**.

correction and pooled by family, the dataset after size correction being intermediate.

Phylogenetic Signal

No clear phylomorphospace can be directly observed using the two first PCs only (**Figure 4**). Nevertheless, the *p*-value resulting from the permutation test, testing the phylogenetic signal on the plotting area of the shape variation, is significant considering the original dataset and the dataset of the stapes after size effect correction without pooling by family (*p*-value = 0.0031 and *p*-value = 0.0029, respectively, **Supplementary Data S3**). It is highly significant when testing the phylogenetic signal on the datasets after size effect correction and pooled by family (*p*-value = 0.0008). It indicates that we can reject the null hypothesis of an overall shape variation (with and without size effect) across the tips of the tree which is not different from random rather than being phylogenetically structured. It means that the overall shape of the stapes is phylogenetically informative. The *p*-value resulting from the permutation test testing the phylogenetic signal on the centroid size of the stapes original dataset is also significant (*p*-value = 0.0235). It means that the size of the stapes is related to its phylogeny. Indeed, the two largest specimens from the dataset are Bovidae and the smallest specimens are Tragulidae.

bg-PCA

Bg-PC1 explains 45.51, 45.44, and 47.16% of shape variation associated to the predefined groups (families) for both (**1**) the original dataset (with allometrical signal), (**2**) the dataset without allometrical signal not pooled by family (since a significant correlation between the shape of the stapes and its size exists, and (**3**) the dataset without allometrical signal pooled by family, respectively (**Figure 5**). Bg-PC2 explains 23.66, 23.12, and 23.86% of the three datasets, respectively (**Figure 5**). Clear morphospaces for the different clades can be defined based on the shape of the stapes. Even if some overlap exists, notably between the Bovidae and the Cervidae, clear trends can be observed. The general repartition observed along the bg-PC based on the original dataset and dataset without allometrical signal pooled by family are almost similar with a better segregation of the families in the last analysis (**Figures 5A,C**). Indeed, while the Bovidae mostly plot in the positive values of bg-PC1, the Cervidae are mostly in the negative values in both cases. In these two analyses, the Antilocapridae are among the most negative values along bg-PC1. In all the analyses, the Tragulidae are located around 0 on bg-PC1. A clear separation between Tragulina and Pecora occurs along bg-PC2 of the original dataset and the dataset without allometrical signal pooled by family, the Tragulina being located in the most negative values. Considering the dataset without allometrical signal not pooled by family (dataset 2), the separation between the Bovidae and the Cervidae along bg-PC1 and between the Tragulidae and the Bovidae along bg-PC2 are not clear. It confirms that part of the allometry, deleted in this dataset, provide phylogenetical information. Nevertheless, the mean shape of the different families is relatively similar considering the three datasets.

The stapes of the Tragulidae are distinct being massive with a relatively elongated stapedial footplate and a little elongated stapes capitulum. The crura are relatively parallel and do not directly reach the edge of the stapedial footplate forming a strong angle. The stapedial footplate has a tear shape being antero-posteriorly asymmetrical. The Antilocapridae possess a concave crus stapedis and a shorter posterior crus than the anterior crus with an enlarged stapes capitulum, giving a trapezoidal lateral shape to the bone. The stapedial footplate is very enlarged, ovoid and slightly asymmetrical. The stapedial footplate is also ovoid in stem Pecora. In Cervidae, the crura stapedis are of similar length and straightness with a slightly reduced stapes capitulum. Their stapedial footplate is ovoid and narrow. The Bovidae have a relatively rectangular stapes in lateral view due to relatively straight crura stapedis and an enlarged stapes capitulum. The stapedial footplate is laterally asymmetrical.

Significant and similar results are observed considering the CVA confirming the results observed with the bg-PCA (**Supplementary Data S6**).

DISCUSSION

Allometry in the Stapes

Allometry is one of the main causes known to polarize morphological variation and constrain phenotypic evolution (e.g., Sansalone et al., 2017). Sense organs have been shown to scale negatively with body mass in mammals (Sánchez-Villagra, 2012; Costeur et al., 2019), which has possibly allowed them to evolve very sophisticated hearing capacities. A negative ontogenetic growth allometry is known for the middle ear ossicles including the stapes throughout the deep time evolution of mammals (Luo, 2011). A similar negative allometry at the evolutionary level of species was preliminary observed in a range of extant and extinct mammals (Orliac and Billet, 2016). We show here that the centroid sizes of the stapes and stapedial footplate are correlated with body mass in ruminants with a strong negative allometry (α = 0.1794 and α = 0.1658, respectively). Similar slopes have already been observed using the height of the stapes and the length, width, and the area of the stapedial footplate of large terrestrial mammals as variables against body mass (Fleischer, 1973; Nummela, 1995; Mason, 2001; Orliac and Billet, 2016). The relationship may be different in small size mammals, being more isometric (Nummela, 1995; Mason, 2001). Differences are also observed depending of the ecology of the animal. Subterranean and aquatic mammals, where the acoustic environment is different from the surface, possess a significantly enlarged area of the stapedial footplate in comparison to body mass (Nummela, 1995; Mason, 2001).

A negative allometry of size is observed between the centroid size of the stapes and the centroid size of the stapedial footplate (R^2 = 0.9267, *p*-value < 0.0001, α = 0.8901, a isometry values being 1.5, and see **Supplementary Data S2**). An isometric variation of the height of the stapes and the width of the stapedial footplate has been observed in Orliac

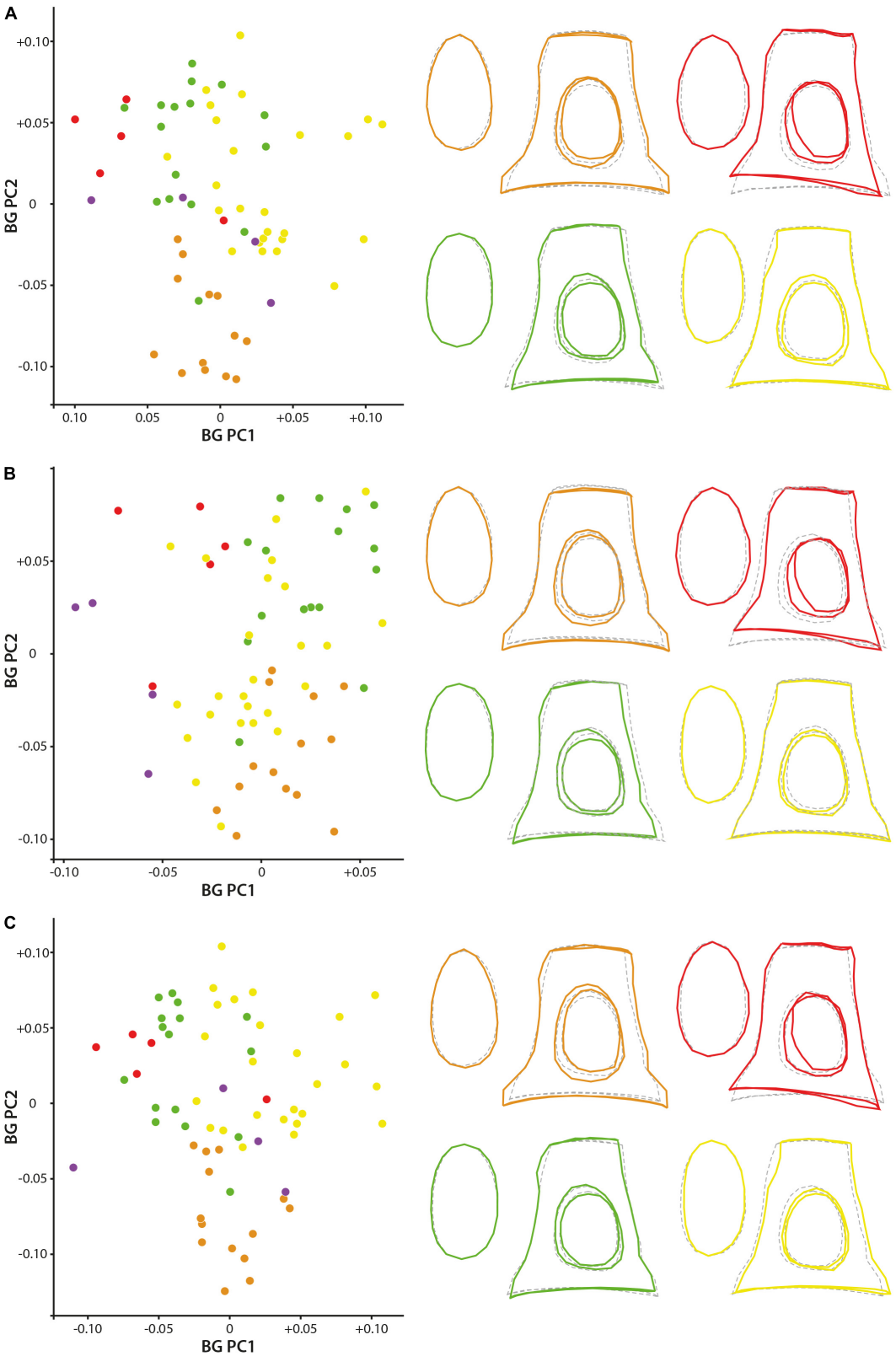

FIGURE 5 | Geometric morphometric bg-PCA results. **(A)** stapes based on the original 3D landmarks coordinates (dataset 1; PC1 = 45.5%, PC2 = 23.7%), **(B)** dataset without allometrical signal not pooled by family (dataset 2; PC1 = 45.4%, PC2 = 23.1%), and **(C)** dataset without allometrical signal pooled by family (dataset 3; PC1 = 47.2%, PC2 = 23.9%). The mean shape of the Antilocapridae is red, of the Bovidae is yellow, of the Cervidae is green, and of the Tragulidae is orange.

and Billet (2016). The shape of the stapedial footplate may explain such differences. Smaller species of our datatset have a more rounded stapedial footplate while the large ones have more ovoid shapes inducing a smaller relative area. The bony labyrinth shows a negative ontogenetic allometric growth relative to the petrosal bone, to skull length, and to body mass (Billet et al., 2015; Costeur et al., 2017, 2019). It has been demonstrated in ruminants (Mennecart and Costeur, 2016; Costeur et al., 2017) and other placental mammals (e.g., Thean et al., 2017) that bony labyrinth ossification is achieved long before birth, around mid-gestation. The size and weight of the stapes is probably limited by physiological and physical constrains. Nummela (1995) proposed that mammalian tympanic membrane may possess an upper size range to prevent from breakage. Since all the auditory region is highly constrained, this likely imposes an upper size limit to the ossicles in terrestrial mammals (Nummela, 1995), although this hypothesis should be further tested.

The stapedial footplate, the *crura stapedis,* and the *stapes capitulum* form a module. They are subject to similar orientations of strength constrains. The module formed by "intercrural foramens" shows a maximum of covariation. Diamond (1989) hypothesized that "the negative allometry of the stapes imposes an upper limit on the size an animal can reach and still retain a fully developed stapedial artery system" since "with increasing body size, the diameter of the intercrural foramen increases much more slowly than the mass of tissue supplied by the stapedial artery." The intercrural foramens, which are penetrated by the stapedial artery, show a negative allometry in comparison to the stapes centroid size and a clear shape allometry of these structures. It is not clear how long the stapedial artery persists in Ruminantia, it was clearly identified in bovine fetuses (Erdogan and Kilinc, 2012) but its pattern of regression after embryonic stages remains unknown in the group.

Phylogenetic Signal on the Stapes Morphology

The ear region possesses a strong phylogenetic signal (e.g., Schmelze et al., 2005; Quam et al., 2014; Mennecart and Costeur, 2016; Mennecart et al., 2016, 2017; Stoessel et al., 2016a,b; Bastl et al., 2017; Kerber and Sánchez-Villagra, 2018). Stoessel et al. (2016b) noticed that the human stapes differs from the other hominids by its height, a distinct stapedial head, and a specific kidney shape of the footplate, even if the other ossicles may be more phylogenetically informative (Stoessel et al., 2016b). Schmelze et al. (2005) also observed that the ossicles characters help structure the marsupial tree. In particular the stapedial footplate (bullate, flat, or concave), the stapedial ratio, and the overall stapes shape (Schmelze et al., 2005) are phylogenetically informative within the marsupial clade. The marsupial families, and even the Macropodinae subfamily, can be separated based on the association of these three characters only. Orliac and Billet (2016) found that the shape of the stapedial footplate is probably not influenced by allometry. They also suggested that "footplate shape may be examined in order to detect phylogenetically significant

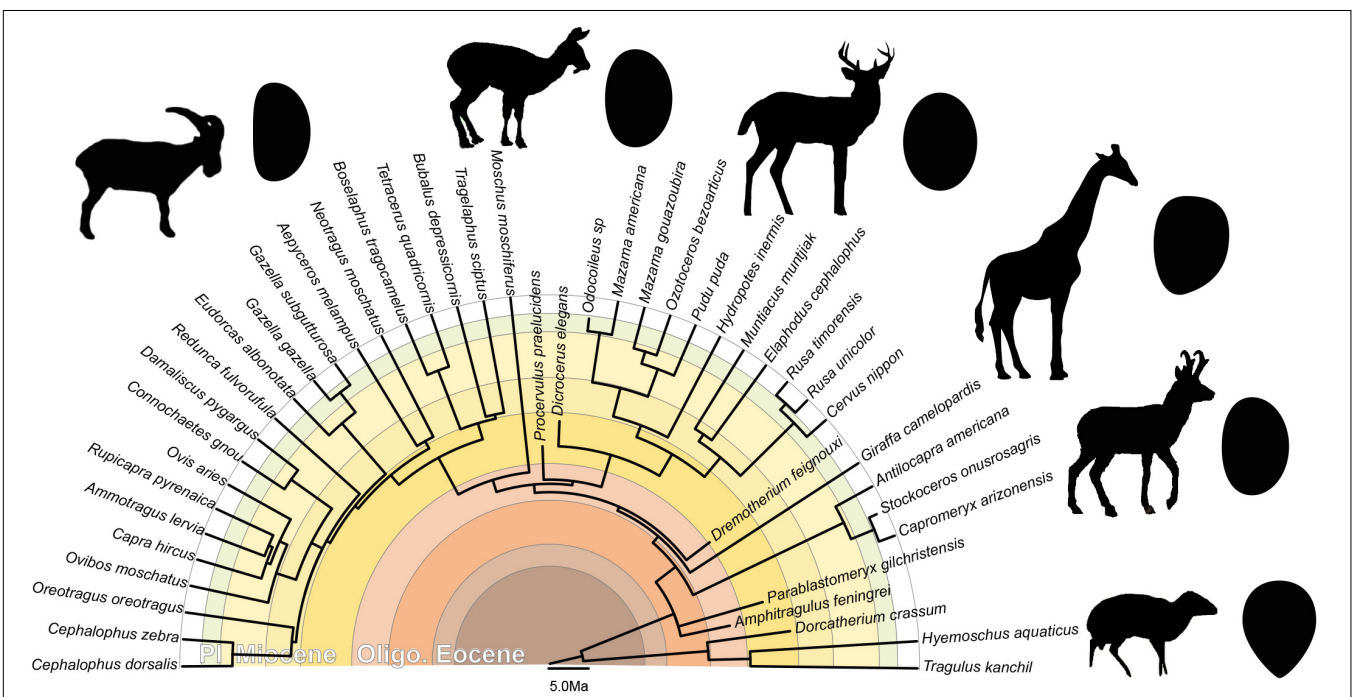

FIGURE 6 | Phylogeny of the studied ruminants with associated general stapedial footplate morphology. Topography of the tree based on (Janis et al., 1998; Hassanin et al., 2012; Mennecart, 2012; and Mennecart et al., 2019; calibration of the Cervidae nodes based on Mennecart et al., 2017; calibration of the Bovidae nodes based on Bibi, 2013). Oligo.: Oligocene; Pl.: Pliocene.

differences between artiodactyl groups (. . .) an elongated stapedial footplate (high footplate ratio) may for example constitute a synapomorphy of the clade Suoidea" (Orliac and Billet, 2016). Mennecart et al. (2017) already proposed that the shape of the stapedial fenestra (the inner ear counterpart of the stapedial footplate) is phylogenetically informative. They noted significant differences within the different Cervidae sub-families. In all considered Cervidae, the stapedial fenestra is ovoid (Mennecart et al., 2017), like the stapedial footplate in the present analysis. However, while the stapedial fenestra is massive in Procervulinae and Dicrocerinae (stem Cervidae), that of Cervinae (crown Cervidae) is elongated (Mennecart et al., 2017). The Capreolinae (crown Cervidae) have an intermediate shape. We here confirm that the stapedial footplate is phylogenetically informative, allowing a distinction between ruminant families. The *p*-values resulting from the permutation test, testing the phylogenetic signal on the plotting area of the shape variation, are significant considering the shape of the stapes with and without size correction (p-value = 0.0031, p-value = 0.0029, and p-value = 0.0008). Shape differences can be observed especially on the stapedial footplate outline (**Figure 6**). The stapedial footplate of Tragulidae has a tear shape being antero-posteriorly asymmetrical. The Cervidae have a symmetrical ovoid stapedial footplate. In Bovidae, the stapedial footplate is laterally asymmetrical. This asymmetry is more marked in larger specimens. These shape differences are already observed in early Miocene representatives making it a good character for family distinction along the ruminant deep time evolution.

CONCLUSION

This first large scale analysis of the ruminant stapes confirms that this bone grows with a negative allometry, as already observed in other mammal groups, i.e., it is relatively larger in smaller species than it is in larger species. This result is in accordance with ontogenetic and evolutionary studies that investigated the growth of sense organs, and in particular of the middle ear bones and bony labyrinth. This result may confirm the role of the middle ear on the evolution of large sizes in mammals since the stapes accommodates a passage for an arterial branch at least in embryonic ontogenetic stages. Regression of the stapedial artery before birth is known in various groups of mammals, especially in primates, but remains largely unknown in ruminants. More work involving dissections may help provide more information on the evolution of sizes in mammals in combination to presence, absence, or regression of the stapedial artery and its impact on the shape of the intercrural foramen. Ideally developmental works in various mammal groups would be essential to model stapedial growth at a large scale. Very much is known in some groups (i.e., primates or some rodents) but virtually nothing in others, such as in Ruminantia. Likewise, investigating the shape of the stapes and of its intracrural foramen in mammals across their evolutionary history, and not only like here within a relatively young clade, may provide information on the evolution of this regression through time. How critical this regression is in terms of hearing abilities is still unknown, although a functional advantage of not having an arterial branch passing through the stapes may be evident in limiting noise (from blood in the artery) transmission to the inner ear. Some mammals are known to keep the stapedial artery through life and this persistence still does not find functional or adaptive explanations.

Our results on the growth and modularity of parts of the stapes highlight under what constraints this critical bone grows and how integrated the ear region in mammals is when stapes shape analysis is compared to the other structures of the ear, i.e., the bony labyrinth, the other ossicles, or the tympanic membrane. Recent evidence has shown that the stapedial fenestra on the bony labyrinth presented a phylogenetic signal, the shape of its counterpart on the stapes, the stapedial footplate, is significant for family determination within Ruminantia, as demonstrated here. Its shape can indeed distinguish families for taxa already known in the early Miocene, when pecoran ruminants started their radiation. Our results confirm recent studies on the stapes itself in other groups of mammals showing that not only the region of the inner ear (bony labyrinth and petrosal bone) is a critical source of phylogenetic data but also that all aspects of the middle ear may provide information. The stapes is small and often falls into the cavity of the inner ear within the petrosal bone. It is therefore often preserved even in long extinct taxa. Its small size makes it a very easy bone to reconstruct from CT-generated data. It is consequently worth looking for in fossil mammal skulls. Although the stapes has been the focus of attention in anatomy for more than 150 years, its morphology in extant mammals is only starting to be investigated on a large taxonomical scale and museum's specimens constitute a great and easily accessible source of data for this bone and for the ear region in general. Our study focused on ruminants highlights the evolutionary and phylogenetic interest of the smallest bone of the mammalian skeleton and provides morphological characters of phylogenetic relevance for future works.

DATA AVAILABILITY STATEMENT

All datasets generated for this study are included in the article/**Supplementary Material**.

AUTHOR CONTRIBUTIONS

BaM and LC designed the study. GS and BeM scanned the specimens. BaM and CG reconstructed the stapes. BaM and LD performed the analyses. All the authors agreed with the manuscript.

FUNDING

This work was supported by the Swiss National Science Foundation (SNF projects 178853, 159854, and 133802).

ACKNOWLEDGMENTS

All our gratitude goes to all the curators and colleagues who provided access to their collection and allowed to scan the specimens. We would like to thank Pip Brewer (Natural History Museum of United Kingdom, London, United Kingdom); Jin Meng, Judith Galkin, Alana Gishlicm and Morgan Hill (American Museum of Natural History, New York, United States); Richard C. Hulbert and Jonathan Bloch (University of Florida, Gainesville, United States); and Yves Laurent and Francis Duranthon (Muséum d'Histoire Naturelle de Toulouse, France). Financial support of the Swiss National Science Foundation is especially acknowledged for financing projects on the ear region (SNF projects 178853 and 159854) the financial support in the frame of the R'equip initiative (133802). BaM warmly thanks Soledad De Esteban-Trivagno (Transmitting Science and ICP), Chris Klingenberg (University of Manchester), and Melissa Tallman (Grand Valley State University) for their precious help in geometric morphometrics through the Transmitting Science program. We would also like to thank the reviewers Paolo Piras, Saverio Bartolini Lucenti, and Antonio Profico for their helpful comments and the editor Pasquale Raia and Luca Pandolfi for inviting us in this special issue.

SUPPLEMENTARY MATERIAL

The Supplementary Material for this article can be found online at: https://www.frontiersin.org/articles/10.3389/feart.2020.00176/full#supplementary-material

DATA S1 | 3D stapes of *Hydropotes inermis* NMB9892.

DATA S2 | Additional figures and measurements.

DATA S3 | Geometric morphometric results for MorphoJ.

DATA S4 | Nexus file of the phylogenetic tree.

DATA S5 | Geometric morphometric results for R.

DATA S6 | Figure and description of the CVA.

REFERENCES

Bastl, K., Nagel, D., and Solé, F. (2017). Incus facet morphology in carnivorous mammals from different ecosystems: taxonomy vs. habitat. C. R. *Palevol* 16, 284–302. doi: 10.1016/j.crpv.2016.11.008

Bernardi, M., and Couette, S. (2017). Eocene paleoecology of *Adapis parisiensis* (Primate. Adapidae): from inner ear to life style. *Anat. Rec.* 300, 1576–1588. doi: 10.1002/ar.23609

Bibi, F. (2013). A multi-calibrated mitochondrial phylogeny of extant Bovidae (Artiodactyla. Ruminantia) and the importance of the fossil record to systematics. *BMC Evol. Biol.* 13:166. doi: 10.1186/1471-2148-13-166

Billet, G., Muizon, C., Schellhorn, R., Ruf, I., Ladevèze, S., and Bergqvist, L. (2015). Petrosal and inner ear anatomy and allometry amongst specimens referred to Litopterna (Placentalia). *Zool. J. Linn. Soc.* 173, 956–987. doi: 10.1111/zoj.12219

Cardini, A., O'Higgins, P., and Rohlf, F. J. (2019). Seeing distinct groups where there are none: spurious patterns from between-group PCA. *Evol. Biol.* 46, 303–316. doi: 10.1007/s11692-019-09487-5

Costeur, L., Mennecart, B., Schulz, G., and Müller, B. (2017). Prenatal growth stages show the development of the ruminant bony labyrinth and petrosal bone. *J. Anat.* 230, 347–353. doi: 10.1111/joa.12549

Costeur, L., Mennecart, B., Müller, B., and Schulz, G. (2019). Observations on the scaling relationship between bony labyrinth, skull size and body mass in ruminants. *Proc. SPIE* 11113:1111313. doi: 10.1117/12.2530702

Costeur, L., Mennecart, B., Schulz, G., and Müller, B. (2016). Middle ear bones of a mid-gestation ruminant foetus extracted from X-ray computed tomography. *Proc. SPIE* 9967:99671Q.

Diamond, M. K. (1989). Coarctation of the stapedial artery: an unusual adaptive response to competing functional demands in the middle ear of some Eutherians. *J. Morphol.* 200, 71–86. doi: 10.1002/jmor.1052000109

Doran, A. H. G. (1878). Morphology of the mammalian ossicula auditus. *Trans. Linn. Soc. Lond.* 1, 371–497. doi: 10.1111/j.1096-3642.1878.tb00663.x

Edgington, E. S. (1987). *Randomization Tests*. New York, NY: Marcel Dekker.

Erdogan, S., and Kilinc, M. (2012). Gross anatomy and arterial vascularization of the tympanic cavity and osseous labyrinth in mid- gestational bovine fetuses. *Anat. Rec.* 293, 2083–2093. doi: 10.1002/ar.21269

Fleischer, G. (1973). Studien am skelett des gehörorgans der säugetiere, einschliesslich des menschen. *Säugetierkd. Mitt.* 21, 131–239.

Fleischer, G. (1978). Evolutionary principles of the mammalian middle ear. *Adv. Anat. Embryol. Cel.* 55, 5–70.

Hammer, Ø, Harper, D. A. T., and Ryan, P. D. (2001). PAST: paleontological statistics software package for education and data analysis. *Palaeontol. Electron.* 4:9.

Hassanin, A., Delsuc, F., Ropiquet, A., Hammer, C., van Vuuren, J. B., Matthee, C., et al. (2012). Pattern and timing of diversification of *Cetartiodactyla* (Mammalia. Laurasiatheria), as revealed by a comprehensive analysis of mitochondrial genomes. *C. R. Biologies* 335, 32–50. doi: 10.1016/j.crvi.2011.11.002

Hyrtl, J. (1845). *Verleichende-anatomische Untersuchungen über das innere Gehörorgan des Menschen und der Säugethiere*. Prague: Friedrich Ehrlich.

Janis, C. M., Scott, K. M., and Jacobs, L. L. (1998). *Evolution of Tertiary Mammals of North America*. New York, NY: Cambridge University Press.

Karachle, P. K., Stergiou, K. I., and Wahl, C. (2012). "4. Morphometrics and allometry in fishes," in *Morphometrics*, (Christina Wahl: IntechOpen), 65–86. doi: 10.5772/34529

Kerber, L., and Sánchez-Villagra, M. R. (2018). Morphology of the middle ear ossicles in the rodent perimys (Neoepiblemidae) and a comprehensive anatomical and morphometric study of the phylogenetic transformations of these structures in *Caviomorphs*. *J. Mamm. Evol.* 26, 407–422. doi: 10.1007/s10914-017-9422-9429

Klingenberg, C. P. (2008). Morphological integration and developmental modularity. *Annu. Rev. Ecol. Evol. Syst.* 39, 115–132. doi: 10.1146/annurev.ecolsys.37.091305.110054

Klingenberg, C. P. (2011). MorphoJ: an integrated software package for geometric morphometrics. *Mol. Ecol. Resour.* 11, 353–357. doi: 10.1111/j.1755-0998.2010.02924.x

Klingenberg, C. P. (2016). Size, shape, and form: concepts of allometry in geometric morphometrics. *Dev. Genes Evol.* 226, 113–137. doi: 10.1007/s00427-016-0539-532

Klingenberg, C. P., and Gidaszewski, N. A. (2010). Testing and quantifying phylogenetic signals and homoplasy in morphometric data. *Syst. Biol.* 59, 245–261. doi: 10.1093/sysbio/syp106

Luo, Z. X. (2007). Transformation and diversification in early mammal evolution. *Nature* 450, 1011–1019. doi: 10.1038/nature06277

Luo, Z. X. (2011). Developmental patterns in Mesozoic evolution of mammal ears. *Annu. Rev. Ecol. Evol. Syst.* 42, 355–380. doi: 10.1146/annurev-ecolsys-032511-142302

Maddison, W. P., and Maddison, D. R. (2010). *Mesquite: a Modular System for Evolutionary Analysis. Version 3.04*.

Maier, W., and Ruf, I. (2016a). Evolution of the mammalian middle ear: a historical review. *J. Anat.* 228, 270–283. doi: 10.1111/joa.12379

Maier, W., and Ruf, I. (2016b). The anterior process of the malleus in *Cetartiodactyla*. *J. Anat.* 228, 313–323. doi: 10.1111/joa.12393

Marriott, F. H. C. (1979). Barnard's monte carlo tests: how many simulations? *Appl. Stat.* 28, 75–77.

Mason, M. J. (2001). Middle ear structures in fossorial mammals: a comparison with non-fossorial species. *J. Zool.* 255, 467–486. doi: 10.1017/s0952836901001558

Meng, J., Yuanqing, W., and Chuankui, L. (2011). Transitional mammalian middle ear from a new Cretaceous Jehol eutriconodontan. *Nature* 472, 181–185. doi: 10.1038/nature09921

Mennecart, B. (2012). The Ruminantia (Mammalia. *Cetartiodactyla*) from the oligocene to the early Miocene of Western Europe: systematics, palaeoecology and palaeobiogeography. *Geofocus* 32, 1–263.

Mennecart, B., and Costeur, L. (2016). A *Dorcatherium* (Mammalia, Ruminantia, middle Miocene) petrosal bone and the tragulid ear region. *J. Vert. Paleontol.* 36:e1211665. doi: 10.1080/02724634.2016.1211665

Mennecart, B., DeMiguel, D., Bibi, F., Rössner, G. E., Métais, G., Neenan, J. M., et al. (2017). Bony labyrinth morphology clarifies the origin and evolution of deer. *Sci. Rep.* 7:13176. doi: 10.1038/s41598-017-12848-12849

Mennecart, B., Rössner, G. E., Métais, G., DeMiguel, D., Schulz, G., Müller, B., et al. (2016). The petrosal and bony labyrinth of Early to Middle Miocene European deer (Mammalia. Cervidae) reveal their phylogeny. *J. Morphol.* 277, 1329–1338. doi: 10.1002/jmor.20579

Mennecart, B., Zoboli, D., Costeur, L., and Pillola, G. L. (2019). On the systematic position of the oldest insular ruminant *Sardomeryx oschiriensis* (Mammalia. Ruminantia) and the early evolution of the Giraffomorpha. *J. Syst. Palaeontol.* 17, 1–14. doi: 10.1080/14772019.2018.1472145

Merchant, S. N., Ravicz, M. E., and Rosowski, J. J. (1996). Acoustic input impedance of the stapes and cochlea in human temporal bones. *Hear. Res.* 97, 30–45. doi: 10.1016/s0378-5955(96)80005-0

Mitteroecker, P., and Bookstein, F. (2011). Linear discrimination, ordination, and the visualization of selection gradients in modern morphometrics. *Evol. Biol.* 38, 100–114. doi: 10.1007/s11692-011-9109-8

Nowak, R. M. (1999). *Walker's mammals of the world, 6th edition*. Baltimore, MD: The John Hopkins University Press.

Nummela, S. (1995). Scaling of the mammalian middle ear. *Hear. Res.* 85, 18–30. doi: 10.1016/0378-5955(95)00030-8

Orliac, M. J., and Billet, G. (2016). Fallen in a dead ear: intralabyrinthine preservation of stapes in fossil artiodactyls. *Palaeovertebrata* 40:e3. doi: 10.18563/pv.40.1.e3

Quam, R. M., Coleman, M. N., and Martinez, I. (2014). Evolution of the auditory ossicles in extant hominids: metric variation in African apes and humans. *J. Anat.* 225, 167–196. doi: 10.1111/joa.12197

R Core Team (2005). *R: A language and environment for statistical computing*. Vienna: R Foundation for Statistical Computing.

Renaud, S., Dufour, A.-B., Hardouin, E. A., Ledevin, R., and Auffray, C. (2015). Once upon multivariate analyses : when they tell several stories about biological evolution. *PLoS one* 10:e0132801. doi: 10.1371/journal.pone.0132801

Rich, T. H., Hopson, J. A., Musser, A. M., Flannery, T. F., and Vickers-Rich, P. (2005). Independent origins of middle ear bones in monotremes and therians. *Science* 307, 910–914. doi: 10.1126/science.1105717

Rosowski, J. J., and Graybeal, A. (1991). What did *Morganucodon* hear? *Zool. J. Linn. Soc.* 101, 131–168. doi: 10.1111/j.1096-3642.1991.tb00890.x

Sánchez-Villagra, M. R. (2012). *Embryos in deep time: the rock record of biological development. Berkeley and*. Los Angeles, CA: University of California Press.

Sansalone, G., Colangelo, P., Kotsakis, T., Loy, A., Castiglia, R., Bannikova, A. A., et al. (2017). influence of evolutionary allometry on rates of morphological evolution and disparity in strictly subterranean moles (Talpinae. Talpidae, Lipotyphla,Mammalia). *J. Mammal.* 25, 1–14. doi: 10.1007/s10914-016-9370-9379

Schlager, S. (2017). "Morpho and Rvcg – Shape analysis in R," in *Statistical Shape and Deformation Analysis*, eds G. Zheng, S. Li, and G. Szekely (Cambridge, MA: Academic Press), 217–256. doi: 10.1016/b978-0-12-810493-4.00011-0

Schmelze, T., Nummela, S., and Sánchez-Villagra, M. R. (2005). Phylogenetic transformations of the ear ossicles in marsupial mammals, with special reference to Diprotodontians: a character analysis. *Ann. Carnegie Mus.* 74, 189–200.

Shingleton, A. (2010). Allometry: the study of biological scaling. *Nat. Educ. Knowled.* 3:2.

Stoessel, A., David, R., Gunz, P., Schmidt, T., Spoor, F., and Hublin, J.-J. (2016a). Morphology and function of neandertal and modern human ear ossicles. *Proc. Natl Acad. U S A.* 112, 11498–11494. doi: 10.1073/pnas.1605881113

Stoessel, A., Gunz, P., David, R., and Spoor, F. (2016b). Comparative anatomy of the middle ear ossicles of extant hominids – introducing a geometric morphometric protocol. *J. Hum. Evol.* 91, 1–25. doi: 10.1016/j.jhevol.2015.10.013

Thean, T., Kardjilov, N., and Asher, R. (2017). Inner ear development in cetaceans. *J. Anat.* 230, 249–261. doi: 10.1111/joa.12548

Tzeng, T. D., and Yeh, S. Y. (1999). Permutation tests for difference between two multivariate allometric patterns. *Zool. Stud.* 38, 10–18.

Wiley, D. (2006). *Landmark Editor 3.6. (Institute for Data Analysis and Visualization*. Davis, CA: University of California.

Wilkie, H. C. (1925). The ossicula auditûs of the sheep (Ovis aries). *J. Comp. Pathol.* 38, 298–301. doi: 10.1016/s0368-1742(25)80051-1

Wilkie, H. C. (1936). The auditory organ of the ox (Bos taurus). *Proc. Zool. Soc. Lond.* 106, 985–1009. doi: 10.1111/j.1469-7998.1936.tb06299.x

Wilson, V. J. (2005). *Duikers of Africa (Masters of the African forest floor)*. Pretoria: Zimbi book.

Conflict of Interest: The authors declare that the research was conducted in the absence of any commercial or financial relationships that could be construed as a potential conflict of interest.

Copyright © 2020 Mennecart, Guignard, Dziomber, Schulz, Müller and Costeur. This is an open-access article distributed under the terms of the Creative Commons Attribution License (CC BY). The use, distribution or reproduction in other forums is permitted, provided the original author(s) and the copyright owner(s) are credited and that the original publication in this journal is cited, in accordance with accepted academic practice. No use, distribution or reproduction is permitted which does not comply with these terms.